Draft version July 19, 2006
Preprint typeset using LaTeX style emulateapj v. 11/26/03

EVOLUTION OF GALAXY LUMINOSITY FUNCTION AND LUMINOSITY FUNCTION BY DENSITY ENVIRONMENT AT $0.03 < Z < 0.5$

Lifang Xia[1,2], Xu Zhou[1], Yanbin Yang[1], Jun Ma[1], Zhaoji Jiang[1]

(Received 2006 April 10; Accepted 2006 July 10)
Draft version July 19, 2006

ABSTRACT

Using galaxy sample observed by the BATC large-field multi-color sky survey and galaxy data of SDSS in the overlapped fields, we study the dependence of the restframe r-band galaxy luminosity function on redshift and on large-scale environment. The large-scale environment is defined by isodensity contour with density contrast $\delta\rho/\rho$. The data set is a composite sample of 69,671 galaxies with redshifts $0.03 < z < 0.5$ and $r < 21.5$ mag. The redshifts are composed by three parts: 1) spectroscopic redshifts in SDSS for local and most luminous galaxies; 2) 20-color photometric redshifts derived from BATC and SDSS; 3) 5-color photometric redshifts in SDSS. We find that the faint-end slope α steepens slightly from -1.21 at $z \sim 0.06$ to -1.35 at $z \sim 0.4$, which is the natural consequence of the hierarchical formation of galaxies. The luminosity function also differs with different environments. The value of α changes from -1.21 at underdense regions to -1.37 at overdense regions and the corresponding M_* brightens from -22.26 to -22.64. This suggests that the fraction of faint galaxies is larger in high density regions than in low density regions.

Subject headings: galaxies: distances and redshifts – galaxies: luminosity function – galaxies: evolution – cosmology: large-scale environment – cosmology: observations

1. INTRODUCTION

Galaxy luminosity function (LF) is a powerful tool in the study of galaxy formation and evolution. Galaxy LF is directly related to galaxy mass function. Press and Schechter (1974) present a simple analytical formula for the mass distribution based on the hierarchical assembly of galaxies. Schechter (1976) gives an emperical functional form for galaxy LF. It has been proposed that it should be universal (Lugger 1986; Colless 1989; Trentham 1998). However, mass function, star-formation process as well as morphological characteristics of galaxies are affected by their environments and evolve with time, galaxy LF is expected to change with time and to vary with galaxy characteristics and the density environments. Deep wide-area sky surveys, such as the Two-Degree Field Galaxy Redshift Survey (2dFGRS; Colless et al. 2001; Norberg et al. 2002) and Sloan Digital Sky Survey (SDSS; York et al. 2000), can generate large samples with a range of redshifts, which are best suited for the mesurment of LF of galaxies. Many studies have been done in galaxy LF by morphological types (Wolf et al. 2003; Cross et al. 2004; Croton et al. 2004), by redshifts (Lilly et al. 1995; Ellis et al. 1996; Wolf et al. 2003; Loveday 2004) and by large-scale environments (Mercurio et al. 2003; Haines et al. 2004; Croton et al. 2004; Hoyle et al. 2003). These enable us to test the theories of formation and evolvement of galaxies in different cosmological models.

Ellis et al. (1996) indicate that there is indeed a steepening in the faint-end slope with redshift. Limited by the size of data sets, however, the evolution of LF to high redshift was not constrained well. For galaxy LF by large-scale environment, analyses reveal that, at low-density environment (Efstathiou et al. 1988; Loveday et al. 1992; Hoyle et al. 2003), the faint-end slope turns out to be $\alpha \sim -1$, and at high-density regions the slope seems to be steeper with $-1.8 < \alpha < -1.3$ (De Propris et al. 1995; Lumsden et al. 1997; Valotto et al. 1997).

In this paper, we use our BATC (Beijing-Arizona-Taiwan-Connecticut) 15 intermediate-band color sky survey data and SDSS 5-color sky survey data to study the evolution of LF and the environmental effects on the LF. BATC photometric system has an average depth of 20.5 mag and the corresponding redshifts of most galaxies are less than 0.3. The SDSS broadband photometric system has an average depth of 23.0 mag with most redshifts less than 0.5. From the investigation in Xia et al. (2002), the accuracy of redshift determination by 15 intermediate-bands, $\sigma_z \sim 0.02$, is much better than that of broad-band, $\sigma_z \sim 0.05$, in the same photometric magnitude errors. Therefore, with the accurate photometric redshifts at $z < 0.3$ and with small $\frac{\Delta z}{z}$ at $0.3 < z < 0.5$, it is possible to combine data of these two systems for accurate measurements of galaxy LF to high redshifts.

The content of this paper is as follows. In § 2 we briefly describe the data sample, the application of photometric redshift code *hyperz* and k-correction. The fitting of galaxy LF and results of LF evolution are given in § 3. Method of environmental classification and results of environmental effects on LF are presented in § 4. § 5 discusses the effects of photometric redshift uncertainty on galaxy LF shape by simulation and summarizes our conclusions. Through out this paper, we assume a ΛCDM cosmological model with matter density $\Omega_m = 0.3$, vacuum density $\Omega_\Lambda = 0.7$, and Hubble constant $H_0 = 100h\mathrm{kms}^{-1}\mathrm{Mpc}^{-1}$ with $h = 0.75$ for the calculation of distances and volumes (see Hogg 1999).

2. DATA

Electronic address: xlf@vega.bac.pku.edu.cn
Electronic address: zhouxu@vega.bac.pku.edu.cn
[1] National Astronomical Observatories, Chinese Academy of Sciences, Beijing, 100012, P. R. China
[2] Department of Astronomy, Peking University, Beijing, 100871, P. R. China

2.1. *Sample*

We use galaxy data including BATC 15-color photometries, SDSS spectroscopies and 5-colors photometries. The BATC Sky Survey performs photometric observations with a large field multi-color system. The observation is carried out with the 60/90 cm f/3 Schmidt Telescope of National Astronomical Observatories, Chinese Academy of Sciences, (NAOC) located at the Xinglong station. For detailed description of survey and performance, see Zhou et al. 2002. The SDSS performs imaging and spectroscopic surveys over π steradians in the northern Galactic cap with a 2.5 m telescope at Apache Point Observatory, Sunspot, New Mexico (York et al. 2000). The detailed description of the photometric and spectroscopic parameters can be found in Stoughton et al. (2002).

We select 17 fields, totally $\sim$ 17 deg^2, observed by BATC and overlapped with SDSS sky survey. Galaxies with the spectroscopic and photometric information in SDSS are obtained from SDSS Data Release 2 (http://www.sdss.org/dr2/). The data of 69,671 galaxies are achieved in SDSS with $r < 21.5$ and $0.03 < z < 0.5$. Galaxies in BATC are selected by coordinates given by BATC and SDSS. 10,681 galaxies in BATC are obtained with the distance deviations in BATC and in SDSS less than $2''.0$. To combine photometries in BATC and SDSS, we need to apply aperture correction to SDSS model magnitudes since that an aperture of 4 pixels (i.e., $r_{\rm ap}$= $6''.8$) is applied in BATC photometries (see details from Yuan et al. 2003). The formula of aperture correction is as below:

$$\Delta m = m_{\rm ap} - m_{\rm model} = -2.5 \log \frac{\int_0^{r_{\rm ap}} 2\pi r I(r) dr}{\int_0^{\infty} 2\pi r I(r) dr} \quad (1)$$

where $m_{\rm ap}$ is the aperture magnitude, $I(r)$ is the profile function of surface intensity for the best fit of de Vaucouleurs or exponential model. For these common galaxies, we estimate photometric redshifts by the total 20 colors.

2.2. *Redshift*

The redshifts in our catalog are measured by three methods. 1,362 galaxies have spectroscopic redshifts observed by SDSS; 10,681 galaxies have photometric redshifts estimated by 20 color photometries consisting of BATC and SDSS; and the rest 57,628 galaxies have photometric redshifts estimated by 5 color photometries of SDSS. The photometric redshift technique is based on SED fitting to estimate redshifts by comparing the spectrum of an object, which should include several strong spectral features such as 4000Å break, Lyman-forest decrement, etc, with the template spectra. We use the *hyperz* program developed by Bolzonella et al. (2000) to estimate redshifts. The accuracy of redshift determination in BATC has been achieved to be 0.02 and the estimated accuracy by broadband filters is about 0.05 (Xia et al. 2002).

The accuracy of photometric redshifts is assessed by galaxies with spectroscopic redshifts in the fields for both systems. Fig. 1 shows the comparision between photometric redshifts and spectroscopic redshifts. We can distinctly see that redshifts of certain amount galaxies are overestimated by the 5-color SDSS photometries. The combined 20 colors can take them back to reasonable estimation. The redshifts in the range from 0.3 to 0.4 seem totally to be overestimated in SDSS, and this may effect the measure of luminosity function dramatically because of the dominant amount of galaxies of SDSS in high redshift layer. The uncertainties are σ= 0.017 for 20-color galaxies and σ= 0.022 for 5-color galaxies with excluding those $\Delta z > 0.05$. Considered that galaxies used to estimate accuracy are bright in magnitudes and accurate in photometries, for faint galaxies, the errors of estimated photometric redshifts should be larger than these estimates. To assess how the uncertainty of photometric redshift affect the predicted luminosity function, we will investigate by simulation in § 5s. Galaxies with $z < 0.03$ are excluded in the construction of galaxy luminosity for the large relative errors for local galaxies. Fig. 2 is the distribution of galaxy redshifts in our composite sample. The first histogram with simple line is the redshift distribution for the total galaxy sample. The second histogram is that for galaxies with 20 colors. And the third histogram with filled area is for galaxies with spectroscopic redshifts. Fig. 2 shows us directly the contributions from these three sources.

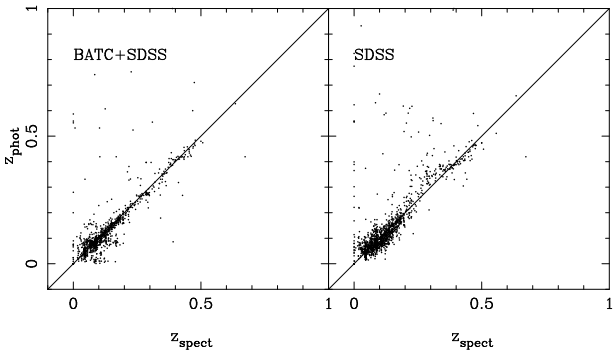

FIG. 1.— The comparison between photometric and spectroscopic redshifts estimated by 20 colors of BATC and SDSS (left panel) and 5 colors of SDSS (right panel), respectively.

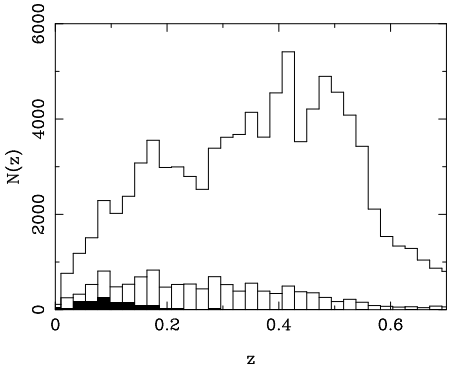

FIG. 2.— Redshift distributions for total galaxies (histogram with simple line), galaxies with 20-color photometric redshifts and galaxies with spectroscopic redshifts (histogram with filled area).

2.3. *k-correction*

By photometric redshifts we calculate absolute magnitudes in the restframe r-band of SDSS:

$$M_r = r - 25 - 5\log d_L(z) - A_r - k(z). \quad (2)$$

where $d_L(z)$ is the luminosity distance in Mpc, A_r is the reddening extinction correction due to intergalactic and interstellar dust scattering and absorption, and $k(z)$ is the k-correction due to the shift of spectrum by redshift. k-correction is significant here since that the sampled redshifts span to high redshifts. The common applied method is to estimate k-correction by galaxy color and morphological type. In the advantage of photometric redshift fitting, we derive k-corrections directly from the spectra templates. In photometric redshift fitting, a best fit template can be achieved for every galaxy, which means the most semblable in the spectrum shape. We modify slightly the code and output the best fit template spectrum at z= 0. Assuming that the observed spectrum has the same k-correction with the best fit template, the k-correction can be corrected directly. The accuracy of this correction is investigated by simulation here.

By the procedure *make_catalog* (see details in Xia et al. 2002), we build a catalog of 1000 galaxies with random types of Bruzual et al. (1993) and redshifts in the range of $z < 0.5$. Totally 20 filters are used. The model k-corrections are output directly from *make_catalog* and the estimated corrections are output by *hyperz*. We, hence, can estimate the accuracy of the k-correction. Fig. 3 shows us the distribution of the corrections with redshifts. The corrections $k(z)$ in the restframe r-band range from 0 to 2 mag. Fig. 4 shows the comparison between model and estimated corrections, and the distribution of the deviations. The rms error of k-correction is about 0.05 mag with a small offset of 0.01 mag.

Reddening extinction is obtained by step fitting in *hyperz* (Xia et al. 2002). The reddening law of Allen (1976) for the Milky Way is adopted. The value of reddening correction is that best fitted by the template spectrum. Here, we also assess the accuracy of the total correction of reddening extinction A_r and k-correction by simulation. It is found that the rms error of this total correction is about 0.08 mag with a small offset of 0.01 mag. In § 5 we will demonstrate by simulation that magnitude error plays the most important role in the prediction of luminosity function and this magnitude error will effect LF fit slightly.

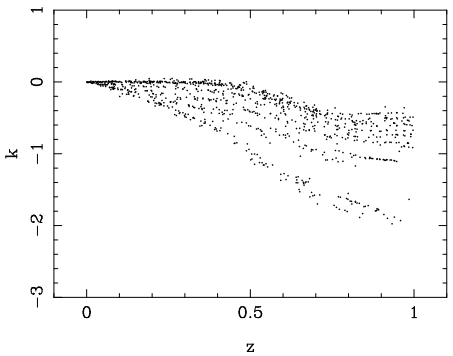

FIG. 3.— The distribution of simulated k-correction with redshifts.

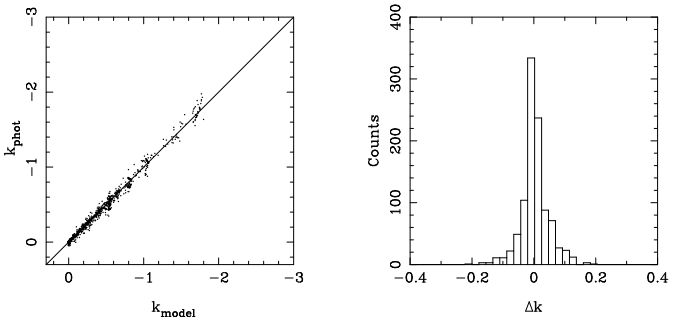

FIG. 4.— Assessment of the accuracy of k-correction and reddening extinction. The left panel is the comparison between model correction and estimated correction. The right panel is the distribution of the deviations.

3. EVOLUTION OF LUMINOSITY FUNCTION

Luminosity function is the number density of galaxies as a function of luminosity. To measure luminosity function, we adopt the approximation of Schechter function (Schechter 1976):

$$\Phi(L)dL = \phi_*(\frac{L}{L_*})^\alpha \exp(-\frac{L}{L_*})d(\frac{L}{L_*}), \quad (3)$$

expressed in the form of per unit absolut magnitude:

$$\Phi(M)dM = 0.4\ln(10)\phi_* 10^{-0.4(M-M_*)(\alpha+1)} \exp[-10^{-0.4(M-M_*)}]dM, \quad (4)$$

where M_* is the characteristic magnitude, i.e., the point at which the bright end cutoff sets in, corresponding to L_*, α is the power-law slope of the faint end, and ϕ_* is the normalization constant. We search these parameters by χ^2 minimization fitting. The fits are performed over the magnitude range $-24 < M_i < -16$ and the normalizations are done in this magnitude range.

To correct the incompleteness arising from the selection effects of distance, the traditional $1/V(M)$ method originally proposed by Schmidt (1968) is implemented in this paper. In the assumption that galaxies distribute homogeneously in comoving space, the correction function is $1/V(M)$, where $V(M)$ is the maximum volume that determined by the maximum distance at which a galaxy with absolute magnitude M can be observed in the apparent magnitude limit. The comoving volume and luminosity distance are calculated as that given by Hogg 1999:

$$dV_C = \frac{c}{H_0}\frac{d_L(z)^2}{(1+z)^2 E(z)} d\Omega dz, \quad (5)$$

$$d_L(z) = (1+z)\frac{c}{H_0}\int_0^z \frac{dz'}{E(z')}, E(z) = \sqrt{\Omega_m(1+z)^3 + \Omega_\Lambda} \quad (6)$$

The structure in small-scale and the possible evolution in number density with redshfit can produce spurious estimate of local LF in this estimator. For the large size of the data set it can partly make up the effect caused by inhomogeneity. For the Malmquist Bias in distance estimates, it origins from that observation effect that greater numbers of galaxies in the univers at greater distances and hence more will have been scattered down

from larger distances than up from smaller ones. We follow the method given by Lynden-Bell et al. (1988) to correct the distance estimates. The correction formula is as below:

$$R = R_e \exp[(\alpha + \frac{1}{2})\Delta^2], \quad (7)$$

where R_e is the estimated luminosity distance D_L, $\alpha = 3$ for uniform distribution, and Δ is the dispersion in $\ln R_e$.

To study the evolution of galaxy LF, we split our galaxy sample into three redshift layers, $0.03 < z < 0.1$, $0.1 < z < 0.3$, and $0.3 < z < 0.5$, with 5,289, 26,162, and 38,220 galaxies respectively. Fig. 5 shows the LFs derived for the three layers $0.03 < z < 0.1$ (filled triangles, solid line), $0.1 < z < 0.3$ (open circles, dot-dashed line), and $0.3 < z < 0.5$ (filled circles, dotted line). The error bars are the errors of poisson counts. Measured parameters are given in Table 1 and the error contours are plotted in the left panel of Fig. 6. As shown in Fig. 5 and Table 1, the faint-end slope α steepens slightly from -1.21 ± 0.02 to -1.25 ± 0.03 and -1.35 ± 0.08 with the increase of redshift. The points appear some discrepancy with Schechter function in bright end. The first point exceeds than expectation. This may result from several reasons. First, it may be due to the observation effects. For the nearest galaxies, the uncertain proper motions can lead to large errors in redshifts and hence overestimate the most luminous galaxies. On the other hand, the amount of intermediate luminous galaxies is much more than that of the most luminous galaxies in the observation, the uncertainty of magnitude and photometric redshift, therefore, can contaminate more intermediate redshift galaxies to low redshifts and then bring to the excess of most luminous galaxies.

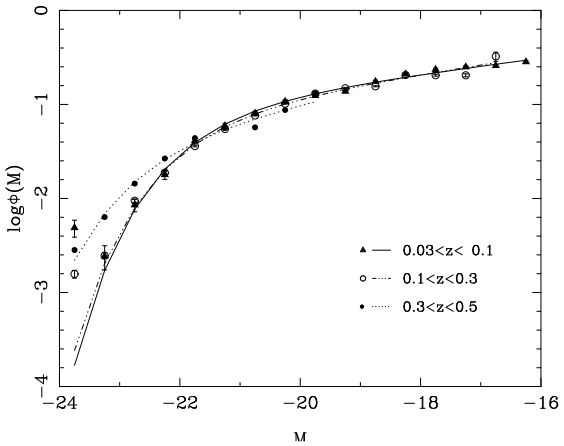

FIG. 5.— The luminosity functions fitted for the three redshift layers $0.03 < z < 0.1$ (filled triangles, solid line), $0.1 < z < 0.3$ (open circles, dot-dashed line) and $0.3 < z < 0.5$ (filled circles, dotted line).

For local galaxies $0.03 < z < 0.1$, $\alpha = -1.21 \pm 0.02$ is consistent with Blanton et al. (2001) $\alpha = -1.20 \pm 0.03$, which is achieved by 11,275 galaxies complete to $r < 17.6$ over 140 deg^2 in SDSS. Blanton et al. (2003) reevaluated galaxy luminosity function at $z = 0.1$ in the $^{0.1}r$ frame by a larger sample of 147,986 galaxies. A much flatter faint-end slope $\alpha = -1.05 \pm 0.01$ was found. This large difference is due to accounting for the evolution of luminosity function in Blanton et al. (2003).

TABLE 1
SHAPE PARAMETERS OF LFS FITTED TO THE THREE REDSHIFT-BINNED SUBSAMPLES AND THAT FITTED TO HIGH AND LOW DENSITY SUBSAMPLES BY DENSITY CONTRAST $\delta\rho/\rho = 30$.

	$\phi_*(\times10^{-2})$	M_*	α_*	χ^2
$0.03 < z < 0.1$/5289	10.16 ± 0.08	-21.80 ± 0.16	-1.21 ± 0.02	0.43
$0.1 < z < 0.3$/26162	8.56 ± 0.13	-21.91 ± 0.12	-1.25 ± 0.03	2.59
$0.3 < z < 0.5$/38220	4.42 ± 0.17	-22.69 ± 0.21	-1.35 ± 0.08	29.77
high/54267	4.14 ± 0.09	-22.64 ± 0.18	-1.37 ± 0.04	10.78
low/15404	8.83 ± 0.05	-22.26 ± 0.16	-1.21 ± 0.04	2.92

From redshift layer $0.1 < z < 0.3$ to $0.3 < z < 0.5$, the estimated faint-end slope is found to change from $\alpha = -1.25 \pm 0.03$ to $\alpha = -1.35 \pm 0.08$. Ellis et al. (1996) constructed lminosity functions using a sample of 1,700 galaxies observed by Autofib Redshift Survey out to $z \sim 0.75$ and gave that α steepens from -1.1 to -1.5 with redshift. Our results is in good agreement with this trend. Loveday (2004) studied the evolution of LF at $z < 0.3$ by a sample of 162,989 spectroscopic galaxies with magnitude limit of $r < 17.6$ in SDSS. The poorly constrained faint-end slope in redshift slice $0.2 < z < 0.3$ is due to the incompleteness in high redshift with a bright magnitude limit $r < 17.6$. loveday04 investigated the effect of different absolute magnitude ranges on the estimated faint-end slope. It is found that the faint-end slope α changes from -1.17 to -2.18 if analysis of redshift slice $0.1 < z < 0.15$ is limited to $M_{0.1_r} < -21.5$. This effect will propbably cause the overestimate of faint-end slope for redshift layer $0.3 < z < 0.5$ in our sample: basically there are no low-luminposity points to tie down the faint end. Though not obvious of the incompleteness for the redshift slice $0.1 < z < 0.3$ in Fig. 5, it could result from an incomplete sample, either.

The estimated characteristic magnitudes $M_* = -21.80 \pm 0.16$, $M_* = -21.91 \pm 0.12$, and $M_* = -22.69 \pm 0.21$ for the three redshift layers, are about 1 to 2 magnitude brighter than previous results (Ellis et al. 1996; Blanton et al. 2001, 2003; Loveday 2004). It is partly due to the different choice of the hubble constant with $h = 0.75$ with others $h = 1$. Another reason comes from the effect of larger magnitude errors and photometric redshift errors than spectroscopic samples. We will demonstrate this effect in § 5.

4. DEPENDENCE OF LUMINOSITY FUNCTION ON ENVIRONMENT

To study the dependence of galaxy luminosity function on large-scale density environment, we subdivide galaxies into high and low density two subsamples according to the density enhancements in three-dimensional redshift space. There are many methods implemented in the literature, here we use the percolation algorithm (Huchra & Geller 1982). This algorithm can search isolate group and cluster. The algorithm identifies every two galaxies by the projected separation D_{12} and the line-of-sight redshift separation z_{12}:

$$D_{12} = \sin(\theta/2)(z_1 + z_2)c/H_0 < D_L(z_1, z_2, m_1, m_2), \quad (8)$$

$$z_{12} = |z_1 - z_2| < z_L(z_1, z_2, m_1, m_2), \quad (9)$$

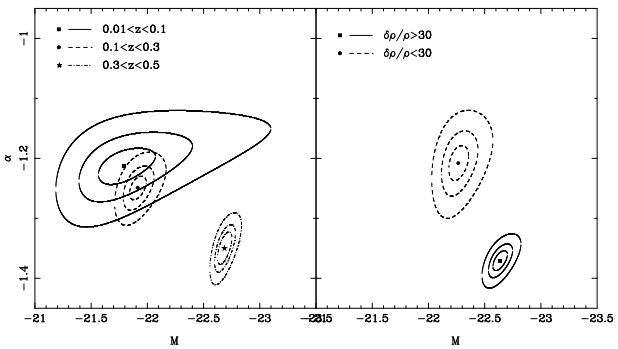

FIG. 6.— 1-σ, 2-σ and 3-σ error contours for parameters M_* and α. Left panel is that for the three redshift layers $0.03 < z < 0.1$ (solid line), $0.1 < z < 0.3$ (dashed line) and $0.3 < z < 0.5$(dot-dashed line) subsamples. Right panel is that for overdense (solid line) and underdense (dot-dashed line) subsamples.

where z_1 and z_2 refer to the redshifts of the two galaxies in the pair, θ is their angular separation, and D_L and z_L are scaled to account for the magnitude limit of the galaxy catalog. All pairs linked by a common galaxy form a group. The limiting number density contrast is

$$\frac{\delta\rho}{\rho} = \frac{3}{4\pi D_0^3}[\int_{-\infty}^{M_l} \Phi(M)dM]^{-1} - 1, \qquad (10)$$

where $\Phi(M)$ is luminosity function, M_l is the faintest absolute magnitude for galaxies with magnitude limit at fiducial distance. For a choosen density contrast and luminosity function (assumed without evolution for the simplicity), the critical distance D_0 can be calculated. Taking into account the decrease of galaxy numbers with increasing distance, link parameter R can be calculated by:

$$R = [\frac{\int_{-\infty}^{M_l} \Phi(M)dM}{\int_{-\infty}^{M_{12}} \Phi(M)dM}]^{1/3}, \qquad (11)$$

In R, M_{12} is the faintest absolute magnitude for a galaxy with magnitude limit at the mean distance of the two galaxies. Then $D_L = RD_0$, and $z_L = Rz_0$. The magnitude limit here is the complete magnitude. The fiducial redshift z_0 we choose is the minimum redshift of the sample, $z_f = 0.03$. D_0 is the fiducial distance corresponding to z_f. $\Phi(M)$ is chosen as that measured by Blanton et al. (2001) for local galaxies by SDSS commissioning data. The LF parameters are: $\phi_* = 1.46 \times 10^{-2} h^3 \mathrm{Mpc}^{-3}$, $M_* = -20.83$, and $\alpha = -1.20$. By this criteria, we can obtained our subsamples by $\delta\rho/\rho$. $\delta\rho/\rho = 30$ is chosen for our classification, with the fiducial distance D_0 corresponding to about 0.35 Mpc. In this scale, the high density subsample includes group galaxies and cluster galaxies (members larger than 5) and low density subsample contains field and void galaxies. We obtain two subsamples with 54,267 and 15,404 galaxies, respectively.

Fig. 7 shows us the luminosity functions derived for subsamples classified by density environment. The discrepancy in fits may be due to the same reason given above. The best-fit Schechter parameters along with the number of galaxies considered in each density environment are listed in Table 1. From Table 1 we can see that, with the enhancement of density, the faint-end slope increases from -1.21 ± 0.04 to -1.37 ± 0.04 and the characteristic magnitude brightens slightly from -22.26 ± 0.16 to -22.64 ± 0.18. The right panel in Fig. 6 shows us the 1-σ (68.3% 2-parameter), 2-σ (95% 2-parameter) and 3-σ χ^2 contours in the $\alpha - M_*$ plane for high and low density populations. The difference is significantly obvious at the confidence level of 95%. Since the curves in Fig. 7 are normalized in the magnitude range $-24 < M_i < -16$, the bright-end density of underdense populations does not mean the numbers of luminous galaxies are larger than that in overdense regions.

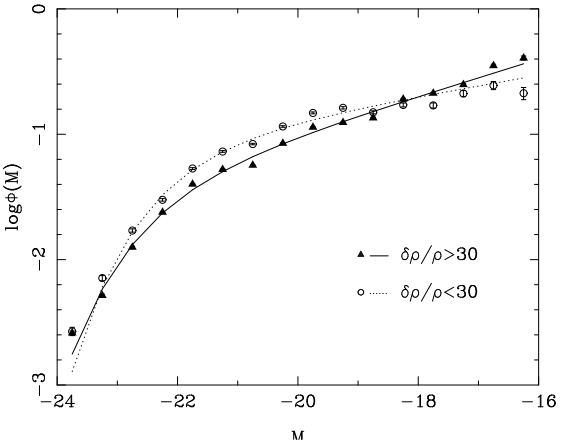

FIG. 7.— Luminosity functions fitted for overdense and underdense subsamples.

Croton et al. (2004) indicates the luminosity function by density environment. They implement galaxies observed by 2dFGRS with median survey depth is $z \approx 0.11$. The local density contrast is determined by δ_8. The same tendency of α is given for regions of different density contrast. In numerical simulations, Mo et al. 2004 studied the dependence of the galaxy luminosity function on large-scale environment in hierarchical cosmology. The results predict that the characteristic luminosity, L^*, increases moderately with density and the faint-end slope is quite independent of density in total. α is virtually constant for late types and increases from -1.3 in underdense regions to -1.8 in overdense regions for early types. Although our samples are not split into subsamples by galaxy types, the predictions are broadly in good agreement. The steepen of the faint-end slope from underdense environment to overdense environment is explained in Tully et al. (2002) by a process of photoionization of the IGM which suppressed dwarf galaxy formation. Overdense regions typically collapse early and can form a dwarf galaxy before the epoch of reionization. Underdense regions, however, collapse later and are thus subject to the photoionization suppression of cooling baryons. The brighten of the characteristic magnitude in dense regions is consistent with the morphology-density relation (Dressler 1980; Binggeli et al. 1988), which is that the population in low density subsamples is dominated by late types and cluster regions have a relative excess of most luminous early-type galaxies. In structure evolution models, it is explained that, the most dense regions of the universe will have collapsed earlier, have larger merger rate and will contain more massive early

type galaxies.

5. DISCUSSION AND CONCLUSION

The uncertainties of galaxy photometric redshifts are about from 0.01 to 0.04 in different photometric magnitude uncertainties. This is the best accuracy achieved by multi-color photometric information. This uncertainty, however, is much bigger than that of spectroscopic redshift, which can be 0.0001. To calculate luminosity function by photometric redshifts, we need to know how the redshift uncertainty and photometric magnitude uncertainty affect the shape of luminosity function. To assess this effect, we perform a series of simulations to fit luminosity function for a galaxy sample distributed as given luminosity function. 100 galaxy samples are created to evaluate the uncertainty of fitted M_* and α. Each sample contains 5000 galaxies homogeneously distributed in the 1 deg^2 cone-shaped comoving space in the redshift range $z < 0.6$. Gaussian distributed photometric errors with $\Delta m = 0.05$, 0.20, 0.50 are assumed. Gaussian distribution with a Gaussian kernel of width $\sigma_z = \hat{\sigma}_z(1+z)$ for photometric redshift erros are adopted, where $\hat{\sigma}_z$ is the redshift rms residual at zero redshift (Fernańdez-Soto et al. 2001; Chen et al. 2003). $\hat{\sigma}_z$ = 0.05, 0.20, and 0.50 are assumed. Here we choose a given luminosity function with $M_* = -21.17$ and $\alpha = -1.26$.

Table 2 lists the estimated rms errors of M_* and α for different photometric uncertainties and redshift uncertainties. We can find that, the faint-end slope α become flatter and the characteristic magnitude M_* become brighter for all uncertainties. It means that the shapes of luminosity function become flatter, which is demonstrated intuitionisticly in Fig. 8. Fig. 8 shows us the luminosity function distribution in Gaussian distributed photometric uncertainties of 0.05 and redshift uncertainties of 0.05 and 0.20. Fig. 9 gives the distribution of M_* and α in the 100 simulations with the same uncertainties as left panel in Fig. 9. From Table 2, with the increase of redshift uncertainties, the characteristic magnitude M_*, is determined with an offset around 0.2 mag brighter and an rms uncertainty about 0.1 mag, and α is determined with an offset around 0.2 flatter and an rms uncertainty about 0.02. The errors become larger with the increase of photometric and redshift uncertainties. We can see by simulation that photometric errors and redshift errors are two major factors for the measurement of luminosity function. This change trends of M_* and α can explain partly the difference between our estimates and previous results.

We study the evolution of galaxy luminosity function in the restfram r-band and the dependence of luminosity function on density environment out to $z \sim 0.5$ by 69,671 galaxies composed by BATC sky survey and SDSS sky survey. We further the depth by photometric redshifts and adopt the Schechter funtion as luminosity function model. The evolution of galaxy luminosity function is studied by three redshift layers $0.03 < z < 0.1$, $0.1 < z < 0.3$ and $0.3 < z < 0.5$. We subdivide the density environment by criteria of isodensity contour. The density contrast is choosen to be $\delta\rho/\rho$= 30. The principle conclusions are summarized as follows:

(i) By simulation we find that photometric uncertainty and redshift uncertainty are two major factors that effect the measurement of luminosity function. In photometric uncertainty of $\Delta m < 0.50$ and redshift uncertainty of $\hat{\sigma_z} < 0.50$, the characteristic magnitude M_*, can be estimated 0.2 mag brighter with a rms error about σ_{M_*}= 0.1; and the faint-end slope α, can be recovered with a factor 0.2 flatter and small uncertainty about σ_α= 0.02.

(ii) There is slight evolution in the shape of galaxy luminosity function with observational depth. We further the accurate measurement of galaxy luminosity function to $z < 0.3$. The faint-end slope steepens slightly from -1.21 to -1.25, -1.35 with the increase of redshift from $0.03 < z < 0.1$ to $0.1 < z < 0.3$, $0.3 < z < 0.5$. The

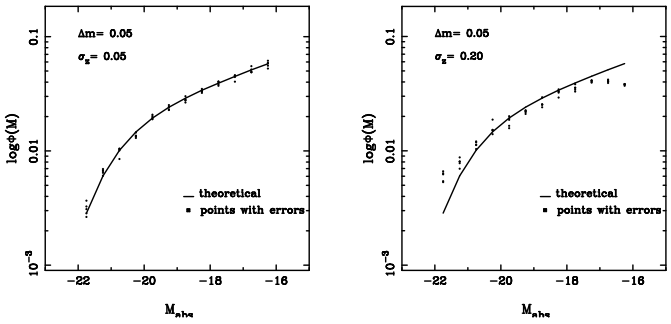

FIG. 8.— Luminosity function distribution of the 100 times simulations in the Gaussian distributed photometric uncertainty of 0.05 and redshift uncertainty of 0.05 and 0.20.

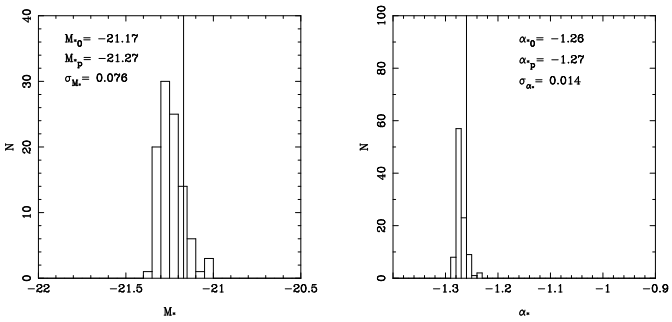

FIG. 9.— Distribution of fitted M_* and α for the simulated samples same as that of left panel of Fig. 8.

TABLE 2
SIMULATED RESULTS OF THE ACCURACY OF LUMINOSITY FUNCTION PARAMETERS IN DIFFERENT MAGNITUDE UNCERTAINETIES AND REDSHIFT UNCERTAINTIES. THE GIVEN PARAMTERS OF LUMINOSITY FUNCTION ARE $M_* = -21.17$ AND $\alpha_* = -1.26$.

$\sigma_{\rm m}$	$\sigma_{\rm z}$	$M_{*,\rm fitted}$	$\sigma_{\rm M_*}$	$\alpha_{*,\rm fitted}$	σ_{α_*}
0.05	0.05	-21.28	0.076	-1.28	0.014
0.05	0.20	-21.53	0.137	-1.19	0.017
0.05	0.50	-21.38	0.123	-0.93	0.022
0.20	0.05	-21.28	0.071	-1.28	0.013
0.20	0.20	-21.53	0.147	-1.21	0.028
0.20	0.50	-21.38	0.120	-0.94	0.023
0.50	0.05	-21.28	0.065	-1.28	0.015
0.50	0.20	-21.53	0.118	-1.18	0.017
0.50	0.50	-21.48	0.117	-0.95	0.028

change of α is broadly consistent with previous claims such as Lilly et al. (1995); Ellis et al. (1996).

(iii) Luminosity function differs distinctly with density environment. The faint-end slope for high density galaxies is steeper than that for low density galaxies. The value of α changes from -1.21 at underdensity regions to -1.37 at high density regions. M_* brightens from -22.26 to -22.64.

We would like to thank the referee Dr. Jon Loveday for his insightful comments and suggestions that improved this paper significantly. We would like to acknowledge very helpful discussions with Zhenyu Wu, Jiuli Li, Zhonglue Wen, Tianmeng Zhang, Jianghua Wu, and Yuzhi Duan. And we would like to thank Dr. David Burstin and Dr. Zuhui Fan for their helpful revision and suggestions over the paper. This work has been supported by the Chinese National Nature Science Foundation, No. 10473012 and 10573020.

REFERENCES

Allen, C. W. 1976, in "Astrophysical Quantities", University of London eds., The Athlone Press, page. 264
Binggeli, B., Sandage, A., & Tammann, G. A. 1988, ARA&A, 26, 509
Blanton, M. R., et al. 2001, AJ, 121, 2358
Blanton, M. R., et al. 2003, ApJ, 592, 819
Bolzonella, M., Miralles, J.-M., & Pelló, R. 2000, A&A, 363, 476
Bruzual, A. G., & Charlot, S. 1993, ApJ, 405, 538
Chen, H.-W., et al. 2003, ApJ, 586, 745
Colless, M. 1989, MNRAS, 237, 799
Colless, M., et al. 2001, MNRAS, 328, 1039
Cross, N. J. G., et al. 2004, AJ, 128, 1990
Croton, D. J., et al. 2004, MNRAS, tmp. 695
De Propris, R., Pritchet, C. J., Harris, W. E., & McClure, R. D. 1995, ApJ, 450, 534
Dressler, A. 1980, ApJ, 236, 351
Efstathiou, G., Ellis, R. S., & Peterson, B. A. 1988, MNRAS, 232, 431
Ellis, R. S., Colless, M., Broadhurst, T., Heyl, J., & Glazebrook, K. 1996, MNRAS, 280, 235
Fernańdez-Soto, A., Lanzetta, K. M., Chen, H.-W., Pascarelle, S. M., & Yahata, N. 2001, ApJS, 135, 41
Haines, C. P., Mercurio, A., Merluzzi, P., Barbera F. La, Massarotti, M., Busarello, G., & Girardi, M. 2004, A&A, 425, 783
Hogg, D. W. astro-ph/9905116
Hoyle, F., Rojas, R. R., Vogeley, M. S., & Brinkmann, J. 2005, ApJ, 620, 618
Huchra, J. P., & Geller, M. J. 1982, ApJ, 257, 423
Lilly, S. J., Tresse, L., Hammer, F., Crampton, D., & Le Fevre, O. 1995, ApJ, 455, 108
Loveday, J., Peterson, B. A., Efstathiou, G., & Maddox, S. J. 1992, ApJ, 390, 338
Loveday, J. 2004, MNRAS, 347, 601
Lugger, P. M. 1986, ApJ, 303, 535
Lumsden, S. L., Collins, C. A., Nichol, R. C., Eke, V. R., & Guzzo, L. 1997, MNRAS, 290, 119
Lynden-Bell, D. et al. 1988, ApJ, 326, 19
Mercurio, A., Massarotti, M., Merluzzi, P., Girardi, M., La Barbera, M., & Busarello, G. 2003, A&A, 408, 57
Mo, H. J., Yang, X. H., Frank C. van den Bosch, & Jing, Y. P. 2004, MNRAS, 349, 205
Norberg, P., et al. 2002, MNRAS, 336, 907
Press, W. J., & Schechter, P. 1974, ApJ, 187, 425
Schechter, P. 1976, ApJ, 203, 297
Schmidt, M. 1968, ApJ, 203, 297
Stoughton, C., et al. 2002, AJ, 123, 485
Trentham, N. 1998, MNRAS, 294, 193
Tully, R. B., Somerville R. S., Trentham N., & Verheijen M. A. W. 2002, ApJ, 569, 573
Valotto, C. A., Nicotra, M. A., Muriel, H., & Lambas, D. G. 1997, ApJ, 479, 90
Wolf, C., Meisenheimer, K., Rix, H.-W., Broch, A., Dye, S., & Kleinheinrich, M. 2003, A&A, 401, 73
Xia, L., et al. 2002, PASP, 114, 1349
Yuan, Q. R., Zhou, X., & Jiang, Zh. J. 2003, ApJS, 149, 53
York, D., et al. 2000, AJ, 120, 1579
Zhou, X., Jiang, Z. J., Xue, S. J., Wu, H., Ma, J., & Chen, J. S. 2001, Chinese J. Astron. Astrophs., 1. 372